Ukrainian Journal of Physical Optics
ISSUE 2
2026

EFFECT OF YTTRIUM DOPING ON THE ELECTRONIC ENERGY STRUCTURE AND OPTICAL PROPERTIES OF GAAS

H. A. ILCHUK [1], O. S. KUSHNIR [2], I. V. SEMKIV [1], S. I. KRUKOVSKYI [1,3], B. ANDRIYEVSKY [4] AND A. I. KASHUBA [1]*

[1] Department of General Physics, Lviv Polytechnic National University, 12 Bandera Street, 79046 Lviv, Ukraine
[2] Department of Optoelectronics and Information Technologies, Ivan Franko National University of Lviv, 107 Tarnavsky Street, 79017 Lviv, Ukraine
[3] Scientific Research Company 'Electron-Carat', 202 Stryiska Street, 79031 Lviv, Ukraine
[4] Faculty of Electronics and Computer Sciences, Koszalin University of Technology, 2 Śniadeckich Street, 75453 Koszalin, Poland
* Corresponding author: andrii.i.kashuba@lpnu.ua

Received: 03.04.2026

Abstract. We report the results for the electronic energy structure of Y-doped GaAs ($Ga_{1-x}Y_xAs$). Its electronic energy spectrum is calculated within the framework of density functional theory. The concentration dependences of the main energy, optical, and structural properties are obtained for a number of yttrium concentrations in the region $x = 0 \div 0.25$. The energy band dispersion and the density of states of these materials are analyzed. Based on the electronic energy spectrum, the real and imaginary components of the dielectric function are calculated. Using the Kramers–Kronig relations, we also derive such fundamental optical functions of $Ga_{1-x}Y_xAs$ as the refractive index n, the extinction coefficient k, and the absorption coefficient α.

Keywords: GaAs, electron energy structure, density of states, band gap, refractive index, optical dielectric function
UDC: 538.9, 535.3
DOI: 10.3116/16091833/Ukr.J.Phys.Opt.2026.02134

1. Introduction

Gallium arsenide (GaAs) finds extensive applications across a diverse spectrum of technologies. In optoelectronics, it remains a cornerstone material for high-efficiency light-emitting diodes [1, 2], laser diodes [3], photodetectors, and photovoltaic devices [4]. Beyond its optical properties, GaAs is indispensable for radio-frequency engineering, particularly in radar and satellite communication systems [5]. Its utility further extends to radiation-hardened solar arrays [6], high-speed integrated circuits [7], and Hall-effect sensors [8].

GaAs crystallizes in a cubic zinc-blende structure described by the space group $F\text{-}43m$ with the lattice constant $a = 5.6537$ Å [9]. It is characterized by a direct band gap, with the appropriate energy $E_g = 1.423$ eV at 300 K [10]. Doping of GaAs and forming appropriate solid solutions enable high-precision modulation of its fundamental electronic and optical parameters. For instance, the fundamental band gap in $Ga_{1-x}Al_xAs$ remains direct at $x < 0.45$ and becomes indirect at $x > 0.45$ [11]. This structural evolution significantly affects the electrical behavior of $Ga_{1-x}Al_xAs$ and, in particular, a conductivity inversion from n- to p-type is observed near $x \sim 0.45$ [12, 13]. These properties facilitate the fabrication of $p+/i/n+$ structures [14]. Alternatively, the structures of this type can be realized through controlled carrier-concentration modulation. To achieve this effect in $Ga_{1-x}Al_xAs$, one has to provide

typical concentrations for the *n*+, *i*, and *p*+ layers of the order of (3÷5)×10^{18}, (1÷2)×10^{17} and (2÷5)×10^{18} cm^{-3}, respectively [15]. Notably, low-level doping (< 0.05 at. %) with rare-earth elements such as Yb, Ce, or Ho also induces the *n*-to-*p*-type inversion [16]. For example, the conductivity of Ce-doped GaAs switches to the *p*-type once the dopant concentration exceeds ~ 0.043 at. % [16]. As a result, doping of GaAs with the rare-earth elements can facilitate the fabrication of novel *p*+/*i*/*n*+ structures with specific characteristics of their electronic spectra. This potential underlines the relevance of the current study.

A density functional theory (DFT) remains one of the primary computational frameworks for investigating the electronic structure of materials [17, 18]. Despite its efficacy, the theoretical data regarding the electronic energy spectrum of Y-doped GaAs is notably scarce if compared to the well-documented properties of pristine GaAs [19]. For instance, although Y-doped GaAs has been examined in Ref. [20], no concentration dependences are reported. Instead, the authors [20] have limited their analysis to a single Y concentration (x = 1/32), which has been studied using the local density approximation for the exchange-correlation potential and ultrasoft pseudopotentials to describe ion-valence interactions.

In the present work, we report on the electronic energy structure of Y-doped GaAs, namely the compounds $Ga_{1-x}Y_xAs$ with the Y concentrations x = 0, 1/32, 2/32, 3/32, and 8/32. The calculations have been carried out within the DFT framework using the generalized gradient approximation (GGA) with the Perdew–Burke–Ernzerhof parametrization for solids, known as PBEsol [21]. The ion-valence interactions have been modeled using norm-conserving pseudopotentials [22]. Application of these computational methods, particularly in the context of Y-doped GaAs, constitutes a methodological novelty of this study. Finally, we have derived the optical properties of Y-doped GaAs from the calculated electronic energy spectrum. In particular, the concentration dependences of the absorption coefficient and the refractive index have been ascertained.

2. Calculation methods

Our DFT-based calculations, including geometry optimization and total energy, electronic spectra, density of states (DOS), and optical properties, were performed using the GGA with the PBEsol parametrization, as described in Ref. [21]. The exchange-correlation functional was integrated with the norm-conserving pseudopotentials to describe, with high precision, the interactions between the ions and the valence electrons (see Ref. [22]).

A plane-wave cut-off energy value E_{cutoff} = 880 eV was taken, which corresponded to the minimum of the total energy. The total energy convergence threshold was set to 5×10^{-6} eV/atom. The Brillouin zone (BZ) integration was performed using a 2×2×2 Monkhorst–Pack **k**-point grid [23]. The initial GaAs structure, with lattice parameters taken from Ref. [9], was subjected to a full geometry optimization. Both the atomic coordinates and the unit cell parameters were refined using a known Broyden–Fletcher–Goldfarb–Shanno algorithm. The optimization procedures proceeded until the residual forces acting on atoms were below 0.01 eV/Å, the maximum atomic displacements were less than 5.0×10^{-4} Å, and the internal stresses did not exceed 0.02 GPa.

$Ga_{1-x}Y_xAs$ compounds with x = 0, 1/32, 2/32, 3/32 and 8/32 were modeled as follows. First, we formed a 2×2×2 supercell of the initial GaAs compound (64 atoms, i.e., $Ga_{32}As_{32}$) based on its already-optimized structure. The next stage involved the theoretical construction of solid-state $Ga_{1-x}Y_xAs$ solutions. In the optimized GaAs structure, Ga atoms

were gradually replaced by Y ones. For such a substitution, the symmetry of the optimized structure GaAs was changed to a triclinic point group *P*1. After that, the crystalline structures of $Ga_{1-x}Y_xAs$ were optimized, and their actual spatial symmetries were found.

3. Results and their discussion

In order to obtain the highest-symmetry cubic structures, only one location of the Y atoms in the structure of 'parent' GaAs has been considered for $Ga_{1-x}Y_xAs$ with x = 0, 1/32, 2/32, 3/32, and 8/32. The optimized structures of our Y-doped GaAs are presented in Fig. 1. For the highest Y concentration x = 0.25, a smaller (1×1×1) unit cell has been used for optimizing the computational efficiency (see Fig. 1). It should be noted that the substitution of Ga with Y atoms leads to a structural transformation from the symmetry *F*-43*m* to *P*-43*m*. The space-group symmetries and the lattice parameters for the optimized structures are summarized in Table 1. Moreover, Table 1 also lists the total energy values for the optimized configurations.

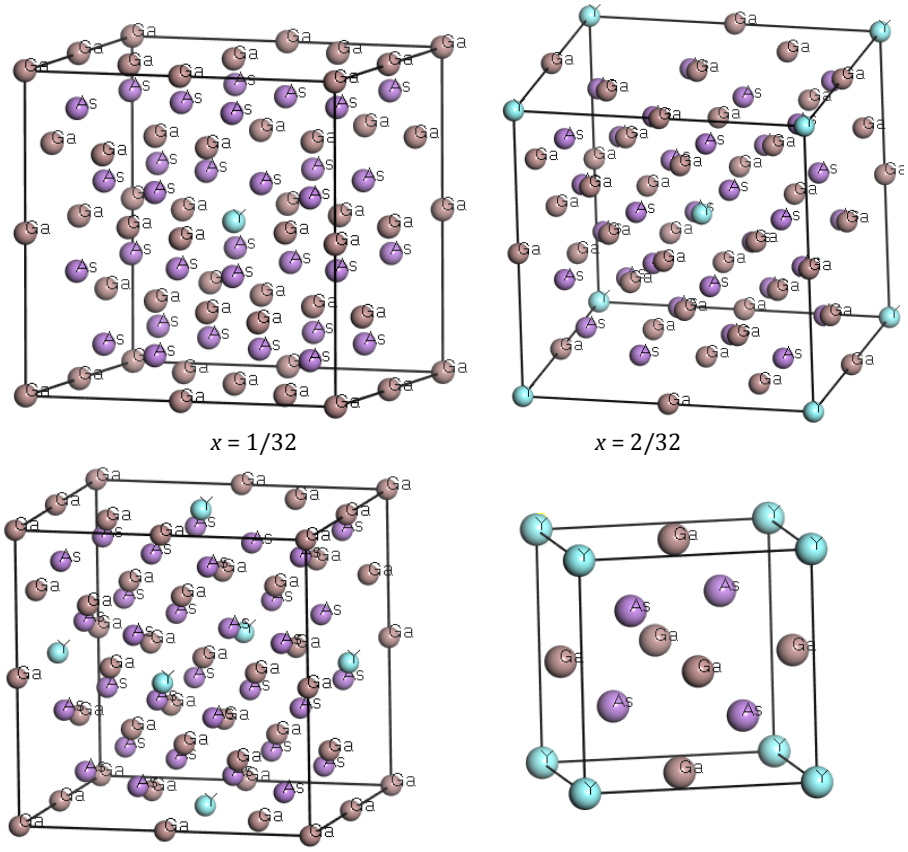

x = 1/32 x = 2/32

x = 3/32 x = 8/32

Fig. 1. Examples of $Ga_{1-x}Y_xAs$ structures obtained after optimization.

Table 1. Structural properties of Y-doped GaAs ($Ga_{1-x}Y_xAs$) after optimization: the abbreviation S. G. implies 'space group'.

x	S. G.	S. G. No	a, Å	V, Å^3	E_{total}, eV	*Supercell*
0	*F*-43*m*	216	5.650075	180.37	–7522.76	1×1×1
1/32	*P*-43*m*	215	11.345824	1460.52	–58519.95	2×2×2
2/32	*P*-43*m*	215	11.389425	1477.42	–56857.93	2×2×2
3/32	*P*-43*m*	215	11.440977	1497.58	–55195.29	2×2×2
8/32	*P*-43*m*	215	5.832139	198.37	–5860.39	1×1×1

According to the structural analysis (see Table 1), the cubic structure is maintained for all of our Y-doped GaAs compounds with the concentrations $x = 1/32$, $2/32$, $3/32$, and $8/32$. However, the space group symmetry is lowered, changing from No. 216 to No. 215. The concentration dependence of the material density for optimized $Ga_{1-x}Y_xAs$ is presented in Fig. 2. Here, an increasing number of Y atoms in the GaAs supercell leads to a decrease in the density.

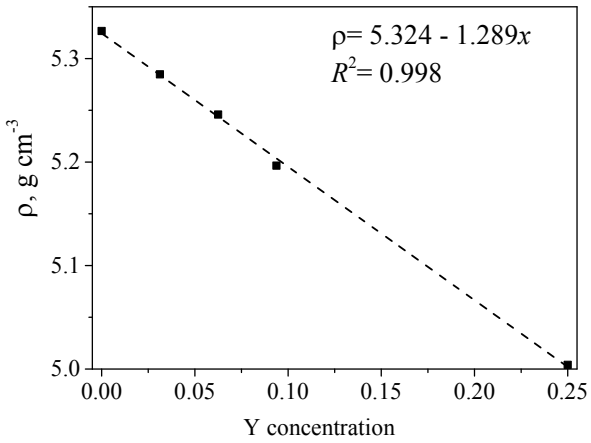

Fig. 2. Concentration dependence of density ρ, as obtained from *ab initio* calculations performed for Y-doped GaAs: dashed line corresponds to a linear fitting.

Fig. 3 shows the calculated electronic energy band diagrams for Y-doped GaAs along the high-symmetry points of the BZ. Note that the calculated electronic band structure and some optical parameters of 'pure' GaAs have already been reported in Ref. [24]. For this reason, we do not present the electronic energy structure and DOS for this canonical semiconducting

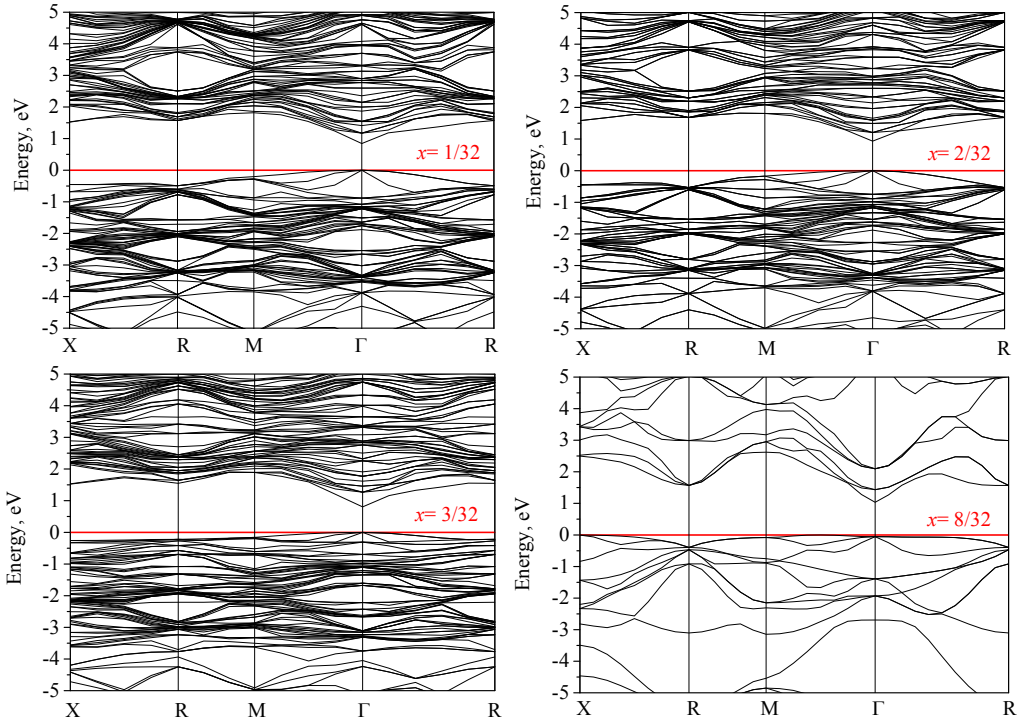

Fig. 3. Electron band energy structures of Y-doped GaAs (see the legend): red lines correspond to Fermi level positions.

compound in this work. Also note that the energy is measured from the Fermi level (E_F= 0 eV). The analysis of our calculation data for the energy band spectrum at x = 0, 1/32, 2/32, and 3/32 shows that the smallest optical band gap is localized in the center of the BZ, i.e. at the point Γ. This means that the corresponding crystals are characterized by a direct energy optical band gap. Unlike these compounds, the minimum energy gap is indirect at the Y-doping level x = 8/32. Nonetheless, the quantitative difference between the indirect optical transition and the direct transition localized at the Γ-point remains less than ~ 0.055 eV (see Table 2).

Table 2. Energy properties of Y-doped GaAs ($Ga_{1-x}Y_xAs$): the indices '*c*' and '*v*' denote the conduction and valence bands, respectively.

x	E_g^{dir}, eV	E_g^{indir}, eV	ΔE, eV	$m_c^{M\text{-}\Gamma\text{-}R}/m_e$	$m_v^{M\text{-}\Gamma\text{-}R}/m_e$
0	0.823	–	–	0.070	0.940
1/32	0.843	–	–	0.413	2.334
2/32	0.935	–	–	0.455	2.784
3/32	0.805	–	–	0.360	3.239
8/32	1.089	1.034	0.055	0.103	1.929

Hence, we infer that doping of gallium arsenide crystallized in a cubic lattice with Y at the largest concentration x = 0.25 induces a change in the minimum band gap from the direct type to the indirect one. As discussed in Section 1, this transition changes the conductivity type from *n*-type at x = 0 to *p*-type at x = 0.25. Therefore, we suppose that Y-doping of GaAs can lead to the formation of $p+/i/n+$ structures, e.g., when using a gradient distribution of the Y impurity through different layers.

Considering the values of the minimum band gap for each studied sample, it can be observed that the band gap width increases with increasing Y concentration in GaAs, except for the concentration x = 3/32. We note that bandgap widths of 0.823 eV and 0.843 eV have been obtained in the present work for GaAs and $Ga_{31}Y_1As_{32}$, respectively. Comparing our theoretical data with the experimental data [10] for pure GaAs (~ 1.423 eV), we find that the calculations performed within the GGA+PBEsol approximation underestimate the bandgap, as it typically happens with all of the theoretical calculations mentioned in Sections 1 and 2. For instance, the bandgap values obtained in Ref. [20] for GaAs and Y-doped GaAs ($Ga_{31}Y_1As_{32}$) are equal to 0.639 eV and 0.625 eV, respectively. One of the reasons for the discrepancy between theory and experiment is that infrared absorption has not been taken into account in our calculations (see explanations in Refs. [18, 21]).

The simplest way to obtain theoretical data that is fully consistent with the experiment is to apply a so-called 'scissors' operator, which shifts the calculated conduction band towards higher energies, thereby increasing the bandgap [18, 21]. Then the calculated conduction band is shifted until the experimental minimum energy gap E_g for the compound under test is achieved. A success of the 'scissors'-operator approach stems from the known Kohn–Sham equations for the band energy dispersion [25].

Regarding the problems discussed above, we note that our results agree better with the experimental data than the theoretical results [20]. Another noteworthy result of the present work is a tendency for the bandgap width to increase with increasing yttrium concentration. On the other hand, a comparison of the data reported by the authors [20] for the only concentration x = 1/32 with their results for pure GaAs indicates the opposite. Although the choice of different computational methods (see Sections 1 and 2) may be a natural reason, we would insist on our data, which are more detailed and concern five different concentrations.

Fig. 3 shows a clear anisotropy in $E(\mathbf{k})$ between the valence and conduction bands. The complex valence top is flatter, which is explained by the fact that holes are less mobile than electrons. This behavior is caused by the inverse relationship between the effective mass of the electron (m_c) / hole (m_v) and the spread $E(\mathbf{k})$ of energy levels [26, 27]:

$$\frac{1}{m^*} = \frac{4\pi^2}{h^2}\frac{\mathrm{d}^2 E(\mathbf{k})}{\mathrm{d}\mathbf{k}^2}, \tag{1}$$

where h is the Planck constant and $E(\mathbf{k})$ denotes the dependence of the band energy E on the electron wave vector $\mathbf{k}$. Table 2 presents the effective masses for Y-doped GaAs determined from the electronic energy band diagrams along different directions in the $\mathbf{k}$-space. The appropriate dependences on the Y concentration are shown in Fig. 4.

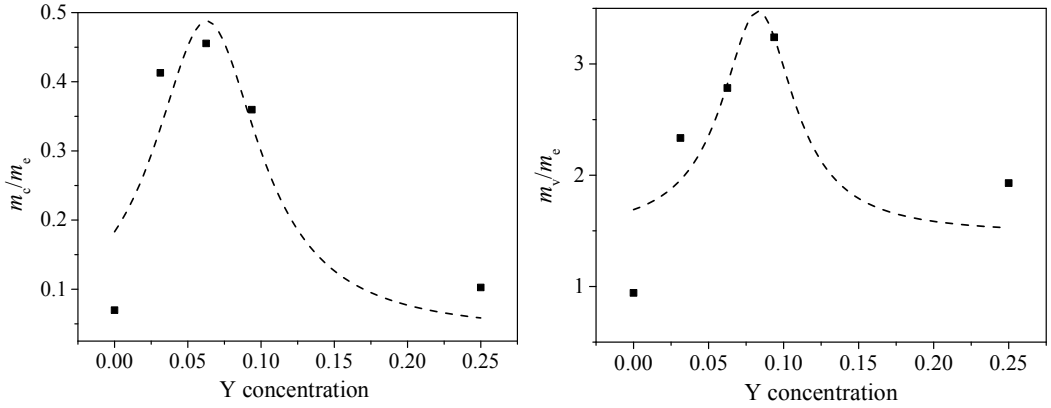

Fig 4. Concentration dependences of the effective masses of electrons (m_c; left panel) and holes (m_v; right panel) for Y-doped GaAs: dash lines are nonlinear fitting with Eqs. (2).

The effective masses of electron ($m_c^{\text{M-Γ-R}} = 0.070m_e$) and hole ($m_v^{\text{M-Γ-R}} = 0.940m_e$) obtained in this work are in good agreement with the known literature data [27]. The dependence of the effective electron mass m_c on the Y concentration in GaAs exhibits a sharp increase in the concentration region $x \sim 2/32$, which is followed by a subsequent decrease. A similar concentration dependence is observed for the effective hole mass, m_v. Note that for the Y-doped GaAs materials with the cubic structure, m_v increases up to the Y concentration $x = 3/32$ and then decreases. Issuing from a characteristic 'bell-like' shape of the concentration dependences of the effective masses of electrons and holes in Y-doped GaAs, one can take the simplest Lorentzian function for the description of these dependences. Then fitting of our m_c and m_v data results in

$$\begin{aligned} m_c^{M-\Gamma-R} &= 0.035 + \left(\frac{0.001}{(x-0.063)^2 + 0.002} \right) \\ m_v^{M-\Gamma-R} &= 1.466 + \left(\frac{0.002}{(x-0.083)^2 + 0.001} \right) \end{aligned}, \tag{2}$$

Based on the electronic energy structure of Y-doped GaAs, we have determined the total and partial electronic DOS (see Fig. 5). The main common features observed across all the x concentrations can be summarized as follows: (i) the energy levels near –15 eV can be attributed to the *d*-states of Ga and As atoms; (ii) the *s*-states of Ga are predominant in the energy region around –10 eV; (iii) the energy levels between –7 and –5 eV are primarily

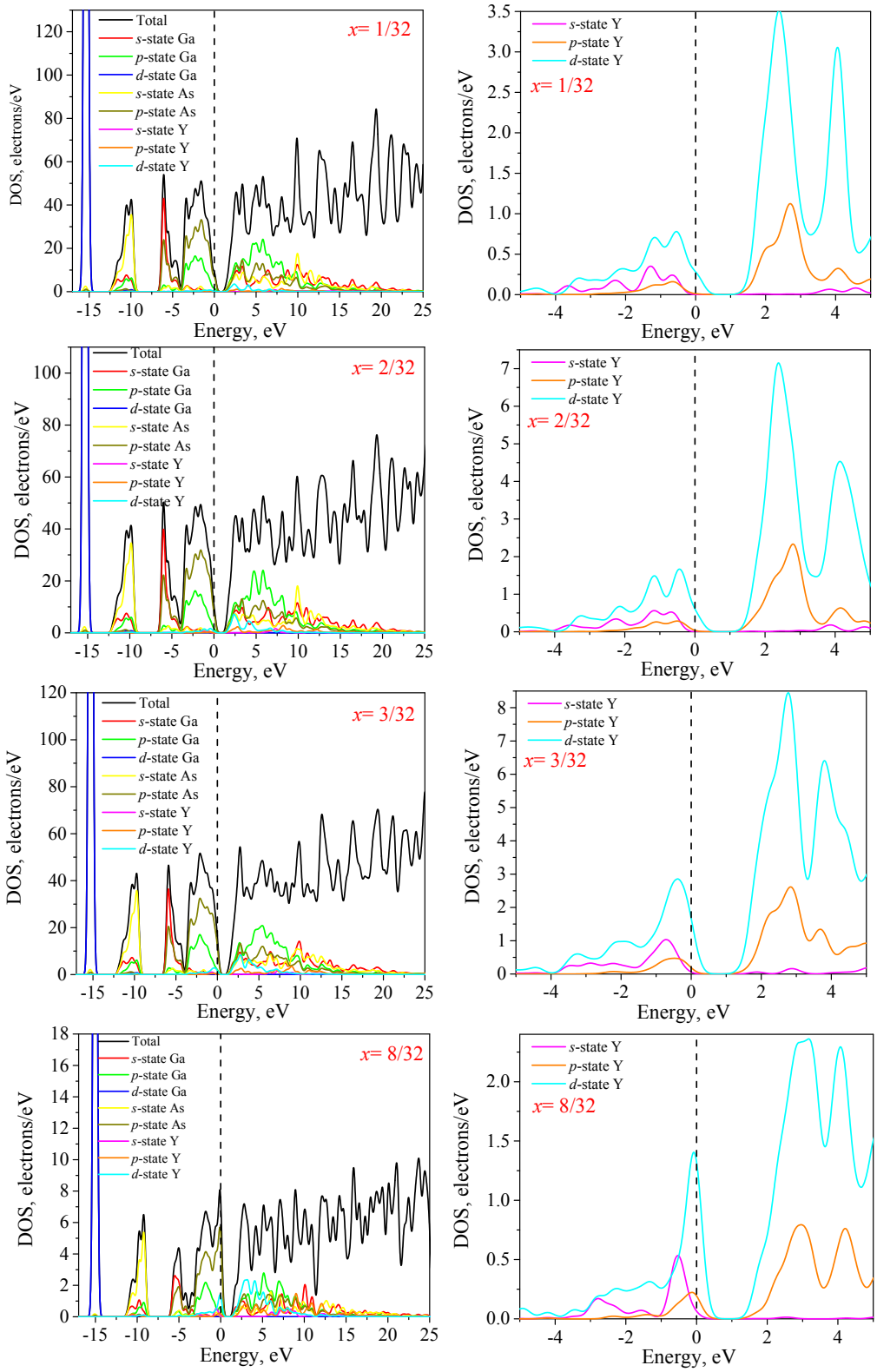

Fig. 5. Total and partial distributions of electronic DOS calculated for $Ga_{1-x}Y_xAs$ with different Y concentrations: right panels correspond to partial distributions of electronic DOS for Y.

composed of *s*-states of Ga; (iv) the maximum of the valence band is formed by the contribution of the *p*-states of As with some admixture of the *p*-states of Ga; (v) the minimum of the conduction band corresponds to the *s*- and *p*-states of Ga and As; (vi) considering the Pauli exclusion principle, we infer that the minimum energy gap is formed by the *s*–*p* transitions with the bond of Ga–As.

In the case of Y-doping of GaAs, the *s*- and *d*-states of Y contribute to the formation of the maximum of the valence band. On the other hand, the *p*- and *d*-states of Y mainly form the minimum of the conduction band (see Fig. 5). Furthermore, we suggest that the transition from the direct band gap to the indirect one at $x = 0.25$ can be attributed to the *d*-states of Y, the density of which increases with increasing yttrium concentration (see Fig. 5).

Based on the electronic energy structures calculated for Y-doped GaAs, one can find the spectral dependences of the real (ε_1) and imaginary (ε_2) parts of the dielectric function $\varepsilon = \varepsilon_1 + i\varepsilon_2$:

$$\varepsilon_1 - 1 = \frac{2}{\pi}\int_0^\infty \frac{t\varepsilon_2(t)dt}{t^2-(\hbar\omega)^2}, \quad \varepsilon_2 = \frac{2e^2\pi}{V\varepsilon_0}\sum_{K,v,c}\left|\left\langle\psi_K^c\left|\hat{u}\cdot r\right|\psi_K^v\right\rangle\right|^2 \delta\left(E_K^c - E_K^v - \hbar\omega\right). \tag{3}$$

In Eqs. (3), E is the energy, $\hat{u}$ the vector of polarization of the incident light, ψ_K^c and ψ_K^v denote the wave functions respectively of the conduction and valence bands in the **k**-space, V is the volume of the unit cell, e the electron charge, ε_0 the dielectric constant in vacuum, r the electron position operator, and $\hbar$ the reduced Planck constant. The spectral dependences of ε_1 and ε_2 are presented in Fig. 6.

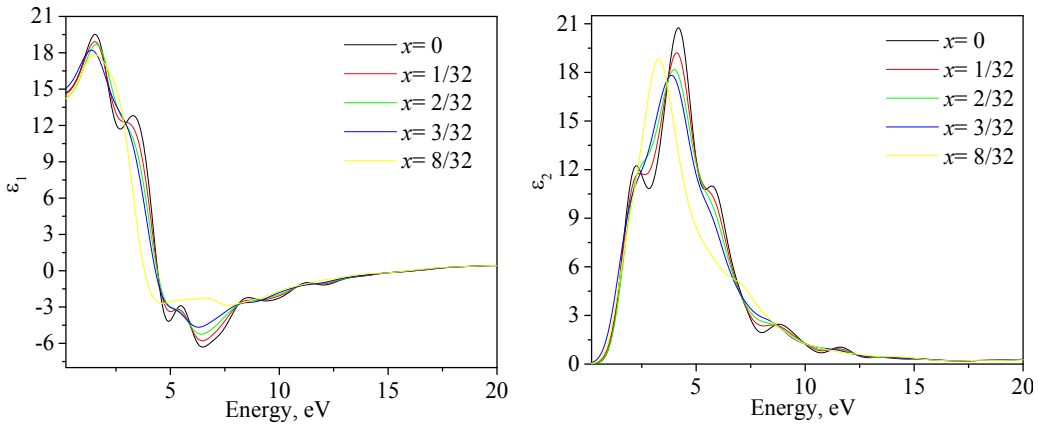

Fig. 6. Real (ε_1) and imaginary (ε_2) parts of the dielectric permittivity ε calculated for $Ga_{1-x}Y_xAs$.

The spectral dependence of the real part ε_1 of complex dielectric permittivity exhibits peaks near 1.5 and 3.3 eV. Furthermore, an increase in ε_1 is observed below ~ 1.5 eV, which is followed by a monotonic decrease above this energy point. The peak at approximately 1.5 eV undergoes a blue shift towards higher energies, with the exception of the concentration $x = 3/32$. The behavior of this peak is analogous to the concentration dependence of the band gap (see Table 2). The peak near 3.3 eV is quenched with increasing Y concentration in GaAs; it is no longer observed at the concentrations exceeding the value $x = 2/32$.

The imaginary part ε_2 of the permittivity exhibits a somewhat more complex spectral behavior. For 'pure' GaAs, three peaks are observed near 2.2, 4.2, and 5.8 eV. The first peak is rapidly quenched upon incorporation of Y into the GaAs matrix. In particular, the peak near

2.2 eV is not detectable at the concentrations $x > 2/32$. In contrast, the peak near 5.8 eV is present for the Y concentrations up to $x = 1/32$. Finally, the main peak located near 4.2 eV at $x = 0$ undergoes a red shift as the Y concentration increases.

Based on the spectral dependences of the ε_1 and ε_2 parameters, one can derive the appropriate dependences for the refractive index n and the extinction coefficient k (see Fig. 7):

$$n = \sqrt{\frac{(\varepsilon_1^2 + \varepsilon_2^2)^{1/2} + \varepsilon_1}{2}}, \quad k = \sqrt{\frac{(\varepsilon_1^2 + \varepsilon_2^2)^{1/2} - \varepsilon_1}{2}}. \tag{5}$$

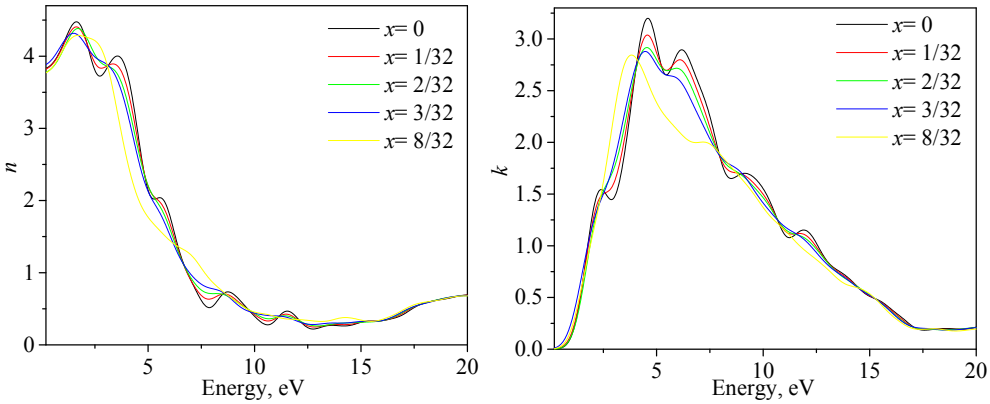

Fig. 7. Refractive index n and extinction coefficient k calculated for Y-doped GaAs.

Note that the spectral dependences of the refractive index and the extinction coefficient are similar to those of the real and imaginary parts of the dielectric permittivity. Finally, the spectral dependence of the absorption coefficient α, which is shown in Fig. 8, has been evaluated as

$$\alpha = 4\pi k / \lambda. \tag{6}$$

Notice that the absolute values of the absorption coefficient calculated by us agree well with the known experimental data [28].

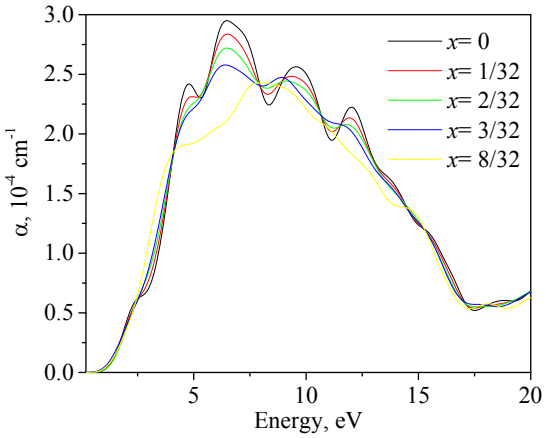

Fig. 8. Absorption coefficient α calculated for Y-doped GaAs.

4. Conclusions

Using the DFT approach, we have calculated the electronic energy structures of the $Ga_{1-x}Y_xAs$ solid solutions at the concentrations $x = 0$, 1/32, 2/32, 3/32, and 8/32. The density of those materials decreases with increasing Y concentration, following a well-defined linear dependence. The analysis of the electronic energy structure reveals that the material with

the Y content $x = 8/32$ is characterized by the indirect optical transitions (E_g^{indir}), whereas $Ga_{1-x}Y_xAs$ at $x = 0$, $1/32$, $2/32$, and $3/32$ shows the direct-band gap transitions (E_g^{dir}). Furthermore, we have analyzed the energy band dispersion, determined by the effective masses of electrons and holes, in Y-doped GaAs.

Based on the electronic energy spectra, we have derived the total and partial DOS for our $Ga_{1-x}Y_xAs$ compounds. It is shown that the band gap is formed by the *s*–*p* transitions associated with the Ga–As bonds. The *d*-states of Y are found to influence the formation of the minimum of the conduction band and the maximum of the valence band. Additionally, we have calculated the spectral dependences of the primary optical functions of Y-doped GaAs, i.e., the real (ε_1) and imaginary (ε_2) parts of the dielectric permittivity ε, the refractive index n, the extinction coefficient k, and the absorption coefficient α.

Funding and acknowledgements. This research was supported by the National Research Foundation of Ukraine under the Project No 2025.07/0258 "Development of novel *p*+/*i*/*n*+ structures based on gallium arsenide thin films". A part of our computer calculations were performed at the ICM of Warsaw University, Poland (the Project No g 104-2591) and the WCSS of the Wrocław University of Technology, Poland (the Project No 053).

Conflict of interest. Authors declare no conflict of interest.

Authors contributions. H. A. Ilchuk: Project administration; original draft writing O. S. Kushnir: Formal analysis; original draft writing; review & editing. I. V. Semkiv: Methodology; visualization. S. I. Krukovskyi: Formal analysis; visualization. B. Andriyevsky: Methodology; original draft writing; supervision. A. I. Kashuba: Conceptualization; original draft writing; review & editing; supervision.

References

1. Takagi, T., Imamoto, H., Sato, F., Imanaka, K., Shimura, M. (1989). High-power broad mesa structure AlGaAs/GaAs single-quantum-well edge-emitting LED. *IEEE Photonics Technol. Lett., 1*, 14–15.
2. Premkumar, M., Arun, M., Sathiya Priya, S., Kalaiarasi, D., Prathipa, R. (2023). Characteristics of gallium arsenide (GaAs) light emitting diode for wireless systems. *Materials Today: Proceedings*, *80*, 1932–1935.
3. Ou, S. S., Yang, J. J., Jansen, M. (1990). 5 W GaAs/GaAlAs laser diodes with a reactive ion etched facet. *Appl. Phys. Lett., 57*, 1861–1863.
4. Dai, X., Zhang, S., Wang, Z., Adamo, G., G. Liu, G., Huang, Y., Couteau, C., Soci, C. (2014). GaAs/AlGaAs nanowire photodetector. *Nano Lett.*, *14*, 2688–2693.
5. Schopf, K. J., Pettenpaul, E. (1994). GaAs amplifiers for radar and mobile communication systems. *Third International Workshop on Integrated Nonlinear Microwave and Millimeterwave Circuits*, 59–67.
6. Yamaguchi, M. (2001). Radiation-resistant solar cells for space use. *Solar Energy Materials and Solar Cells*, *68*, 31–53.
7. Shur, M. (1987) GaAs Digital Integrated Circuits. In: GaAs Devices and Circuits. Microdevices. Springer, Boston.
8. Campesato, R., Flores, C., Passaseo, A., Verni, S. (1992). GaAs Hall sensors made by the MOCVD technique. *Sensors and Actuators A: Physical*, *32*, 651–655.
9. Wyckoff, R. W. G. (1963). ZnS Structure, Sphalerite Structure. *Crystal Structures*, 2nd Ed. Interscience Publishers, New York. *1*, 85–237.
10. El Allali, M., Sørensen, C. B., Veje, E., Tidemand-Petersson, P. (1993). Experimental determination of the GaAs and $Ga_{1-x}Al_xAs$ band-gap energy dependence on temperature and aluminum mole fraction in the direct band-gap region. *Phys. Rev. B*, *48*, 4398.
11. Adachi, S. (1994). GaAs and Related Materials. World Scientific: Singapore.
12. Temkin, H., Keramidas, V. G. (1980). Room-temperature conductivity and the band structure of *n*-$Ga_{1-x}Al_xAs$. *J. Appl. Phys.*, *51*, 3269–3272.
13. Hava, S., Hunsperger, R. (1985). Thermoelectric properties of $Ga_{1-x}Al_xAs$. *J. Appl. Phys.*, *57*, 5330–5335.
14. Mil'shtein, S., Halilov, S. (2018). Cascaded $Ga_{1-x}Al_xAs$/GaAs solar cell with graded *i*-region. *AIP Conf. Proc.*, *1934*, 020004.
15. Krukovskyi, S. I., Ilchuk, H. A., Krukovskyi, R. S., Semkiv, I. V., Zmiiovska, E. O., Tokarev, S. V. (2018). Formation of graded-gap active region of the photoelectric converter based on AlGaAs solid solutions by trimethylaluminium flow modulation in the MOC vapour deposition method. *Journal of Nano and Electronic Physics*, *10*, 03025.

16. Krukovskyi, S., Krukovskyi, R., Ilchuk, H., Zmiiovska, E., Semkiv, I. (2018). Formation of GaAs/AlGaAs epitaxial layers, with gradient profiles of charge carrier distribution. *14th International Conf. on Advanced Trends in Radioelectronics, Telecommunications and Computer Eng., TCSET-2018 Proc.*, 462–465.
17. Ilchuk, H., Zmiiovska, E., Petrus, R., Semkiv, I., Lopatynskyi, I., Kashuba, A. (2020). Optical properties of CdMnTe film: experimental and theoretical aspects. *Journal of Nano- and Electronic Physics*, *12*, 01027.
18. Rudysh, M. Ya. (2022). Electronic structure, optical and elastic properties of $AgAlS_2$ crystal under hydrostatic pressure. *Materials Science in Semiconductor Processing*, *148*, 106814.
19. Baldereschi, A., Maschke, K., Hess, E., Neumann, H., Schulze, K.-R., Unger, K. (1977). Energy band structure of $Al_xGa_{1-x}As$. *J. Phys. C: Solid State Phys.*, *10*, 4709.
20. Deng, Y., Zhang, C., Qin, X., Yan, W. (2025). Electronic structure and optical properties of GaAs doped with rare-earth elements (Sc, Y, La, Ce, and Pr). *Crystals*, *15*, 98.
21. Perdew, J. P., Ruzsinszky, A., Csonka, G. I., Vydrov, O. A., Scuseria, G. E., Constantin, L. A., Zhou, X., Burke, K. (2008). Restoring the density gradient expansion for exchange in solids and surfaces. *Phys. Rev. Lett.*, *100*, 136406.
22. Hamann, D. R., Schlüter, M., Chiang, C. (1979). Norm-conserving pseudopotentials. *Phys. Rev. Lett.*, *43*, 1494.
23. Monkhorst, H. J., Pack, J. D. (1976). Special points for Brillouin-zone integrations. *Phys. Rev. B*, *13*, 5188.
24. Ilchuk, H. A., Semkiv, I. V., Krukovskyi, S. I., Andriyevsky, B., Kashuba, A. I. (2026). Concentration dependences of electronic band structure of La-doped GaAs. *Journal of Physics Communications* (submitted).
25. Kohn, W., Sham, L. J. (1965). Self-consistent equations including exchange and correlation effects. *Phys. Rev.*, *140*, A1133.
26. Kashuba, A. (2023). Influence of metal atom substitution on the electronic and optical properties of solid-state $Cd_{0.75}X_{0.25}Te$ (X = Cu, Ag and Au) solutions. *Physics and Chemistry of Solid State*, *24*, 92–101.
27. Nakwaski, W. (1995). Effective masses of electrons and heavy holes in GaAs, InAs, A1As and their ternary compounds. *Physica B*, *210*, 1–25.
28. Akinlami, J. O., Ashamu, A. O. (2013). Optical properties of GaAs. *J. Semicond.*, *34*, 032002.

Ilchuk, H. A., Kushnir, O. S., Semkiv, I. V., Krukovskyi, S. I., Andriyevsky, B., Kashuba, A. I. (2026). Effect of Yttrium Doping on the Electronic Energy Structure and Optical Properties of GaAs. *Ukrainian Journal of Physical Optics*, *27*(2), 02134 – 02144.
doi: 10.3116/16091833/Ukr.J.Phys.Opt.2026.02134

Анотація. *Представлено результати дослідження електронної енергетичної структури GaAs, легованого Y ($Ga_{1-x}Y_xAs$). Його електронний енергетичний спектр розраховано в рамках теорії функціоналу густини. Концентраційні залежності основних енергетичних, структурних і оптичних властивостей $Ga_{1-x}Y_xAs$ встановлено для деяких концентрацій Y у діапазоні $x = 0 \div 0{,}25$. Проведено аналіз дисперсії енергетичних зон і густини станів цих матеріалів. На основі електронного енергетичного спектру розраховано дійсну та уявну складові діелектричної функції. Використовуючи співвідношення Крамерса–Кроніга, одержано фундаментальні оптичні функції, такі як показник заломлення n, коефіцієнт екстинкції k і коефіцієнт поглинання α.*

Ключові слова: *GaAs, електронна енергетична структура, густина станів, заборонена зона, показник заломлення, оптична діелектрична функція*